

Exploring Charge Density Waves in two-dimensional NbSe₂ with Machine Learning

Norma Rivano,^{1,*} Francesco Libbi,¹ Chuin Wei Tan,¹ Christopher Cheung,² Jose Lado,³ Arash Mostofi,² Philip Kim,⁴ Johannes Lischner,² Adolfo O. Fumega,^{2,3,†} Boris Kozinsky,^{1,‡} and Zachary A. H. Goodwin^{1,2,5,§}

¹*John A. Paulson School of Engineering and Applied Sciences, Harvard University, Cambridge, MA 02138, USA*

²*Departments of Physics and Materials and the Thomas Young Center for Theory and Simulation of Materials, Imperial College London, London SW7 2AZ, United Kingdom*

³*Department of Applied Physics, Aalto University, 02150 Espoo, Finland*

⁴*Department of Physics, Harvard University, Cambridge, Massachusetts 02138, USA*

⁵*Department of Materials, University of Oxford, Parks Road, Oxford OX1 3PH, United Kingdom*

Niobium diselenide (NbSe₂) has garnered attention due to the coexistence of superconductivity and charge density waves (CDWs) down to the monolayer limit. However, realistic modeling of CDWs—accounting for effects such as layer number, twist angle, and strain—remains challenging due to the prohibitive cost of first-principles methods. To address this, we develop machine learning interatomic potentials (MLIPs), based on the Allegro architecture—an E(3)-equivariant model—specifically tailored to capture subtle CDW effects in NbSe₂. These MLIPs enable efficient exploration of commensurate and incommensurate CDW phases, as well as the dimensional dependence of the transition temperature, evaluated using the Stochastic Self-Consistent Harmonic Approximation (SSCHA). Our findings reveal a strong sensitivity of CDWs to stacking and layer number, and a slight suppression of the transition temperature with increasing thickness. This work opens new possibilities for studying and tuning CDWs in NbSe₂ and other 2D systems, with implications for electron-phonon coupling, superconductivity, and advanced materials design.

Niobium diselenide (NbSe₂) has long been studied for its unique interplay between charge density wave (CDW) order and superconductivity, which persists even in the monolayer limit [1, 2]. As a van der Waals material, NbSe₂ can be exfoliated into monolayers and multilayers, providing an ideal platform for studying dimensionality-dependent phenomena. [2–12] Unlike quasi-one-dimensional materials, where CDWs arise from Fermi surface nesting [13–16], two-dimensional (2D) NbSe₂ lacks such features. Instead, electron-phonon coupling (EPC) has emerged as the primary driver of CDW formation, accompanied by periodic lattice distortions. [6, 7, 17, 18] Understanding CDWs and their connection to EPC is essential for uncovering the microscopic mechanisms of superconductivity [7, 19–22], opening avenues for novel technological applications [23–27].

Because of the intricacy of the translation symmetry breaking in 2D materials, CDWs remain an active area of investigation. [2, 4, 5, 8, 9, 17, 21] While reduced dimensionality can strengthen CDWs [9], it may also introduce fluctuations that disrupt long-range order [28] in the sense of the Mermin-Wagner theorem. In monolayer NbSe₂, a 3×3 CDW with a transition temperature of up to 145 K [1, 2] has been observed, significantly higher than the bulk value of 33 K [1]. However, other studies report weaker dimensionality dependence, with transition temperatures around 73 K [11] and 45–25 K [29]. Several density-functional theory (DFT) studies [30–32] have identified multiple 3×3 phases in monolayers, with

the ‘hollow’ phase, where Nb atoms displace toward the center of the hexagonal unit cell (see Fig. 2a), best matching experimental measurements [30].

Beyond dimensionality, CDWs are highly sensitive to factors like strain [3], doping [3, 24], stacking order [33] and substrates [34]. Moreover, moiré superlattices, created by introducing twist angles between 2D materials, offer a promising platform to further tune and discover new properties. [35–44] Despite growing interest, many questions remain open: How do CDWs stack in multilayers? How can different CDW phases coexist? How does the transition temperature depend on dimensionality? What role do environmental factors play? Answering these questions remains computationally prohibitive with current first-principles methods. The modulation of CDWs in multilayer and moiré systems is still poorly understood [44, 45], and simulating these systems remains challenging [46].

To address the complexity of CDWs in realistic environments, we turn to machine learning interatomic potentials (MLIPs), a powerful alternative for simulating large systems with high fidelity and reduced computational costs [47–51]. While MLIPs have been developed for various 2D materials and transition metal dichalcogenides (TMDs) [52–54], none are specifically tailored for CDWs in NbSe₂. This is a particularly difficult case, as commensurate CDWs typically involve periodic lattice distortions (~0.1 Å) accompanied by energy changes of the order of 1 meV/atom, testing the accuracy limits of current MLIPs.

In this study, we develop an approach for training accurate and transferable MLIPs using the state-of-the-art Allegro architecture [56], designed to model both normal and CDW phases. We aim to establish a unified potential for exploring CDW order in mono- and bilayers,

* Corresponding author: nrivano@g.harvard.edu

† Corresponding author: adolfo.oterofumega@aalto.fi

‡ Corresponding author: bkoz@seas.harvard.edu

§ Corresponding author: zac.goodwin@materials.ox.ac.uk

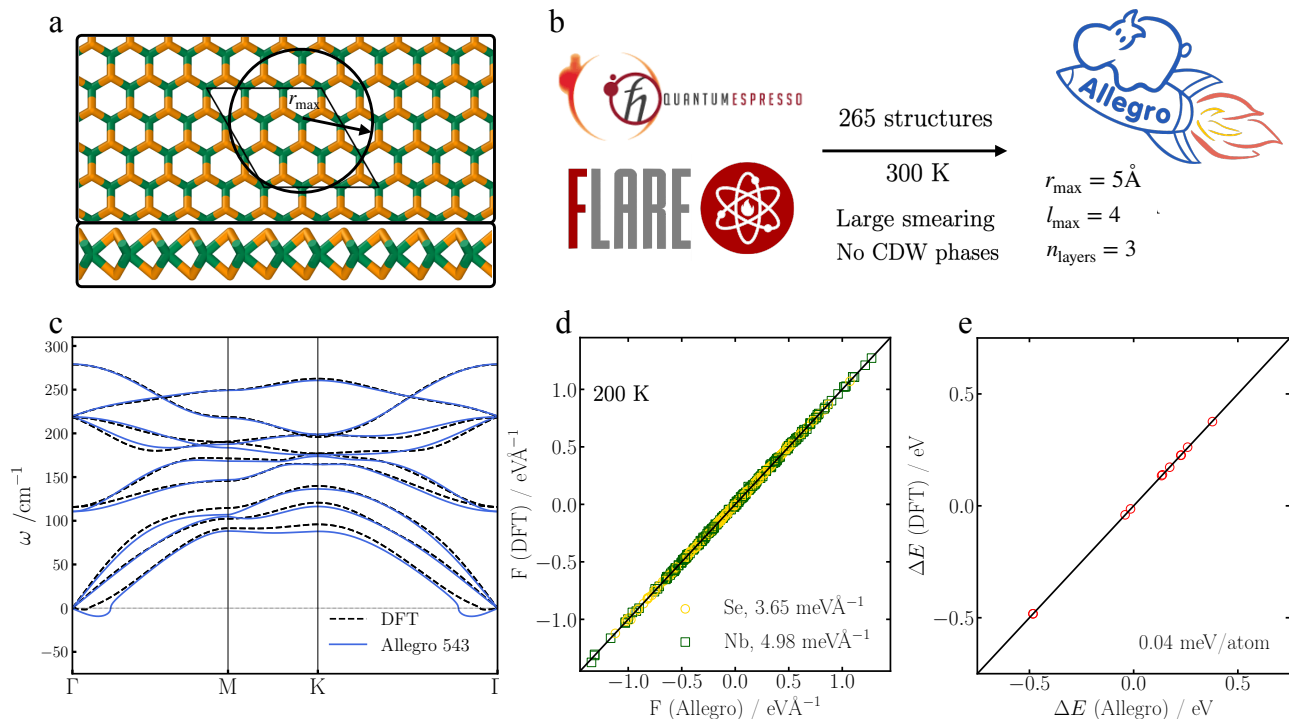


Figure 1: Development of a machine-learned interatomic potential (MLIP) for NbSe₂ in the normal state (large smearing, no CDW). **a** - Structure of monolayer NbSe₂ in the normal phase, visualized using Ovito [55], showing a 3×3 supercell. Orange sticks represent Se atoms, and green sticks represent Nb atoms. The range of interactions ($r_{\max} = 5 \text{ \AA}$) is indicated schematically. **b** - Computational workflow employed to develop the MLIP. **c** - Phonon dispersion relations computed using DFT + Phonopy and Allegro MLIP + Phonopy, demonstrating close agreement. **d** - Force mean absolute error (MAE) from molecular dynamics (MD) simulations at 200 K in the NVT ensemble; values are reported per element as shown in the legend. **e** - Corresponding energy MAE per simulation frame. See Supporting Information (SI) for additional computational details.

while creating an optimized protocol—for hyperparameters and datasets—that can be extended to other 2D CDW systems. We validate our approach by comparing structural and phonon calculations from molecular dynamics (MD) simulations with DFT results. Special attention is given to testing the MLIPs in both commensurate and incommensurate supercells, crucial for modeling moiré systems. Our results highlight the sensitivity of CDWs to factors like number of layers, stacking, and incommensurability, with significant implications for EPC and superconductivity.

Owen *et al.* [57] showed that potential energy surfaces of certain transition metals, including Nb, are very sensitive functions of atomic positions due to the sharply varying density of d-states near the Fermi energy. This sensitivity requires high angular resolution to capture complex many-body interactions, making these materials challenging even for state-of-the-art neural equivariant MLIPs [58]. As 2D NbSe₂ is metallic with d-orbital-dominated states near the Fermi level [30], constructing an accurate MLIP is nontrivial. We begin by training a model for the monolayer in the normal phase, using large electronic smearing (effective electronic temperature). This simplifies the energy landscape, suppresses

the CDW, and stabilizes the normal state, aiding the development of a robust potential energy surface model.

In the normal state, monolayer NbSe₂ consists of a triangular lattice of Nb atoms bonded to 6 Se atoms. Se atoms form triangular lattices above and below the Nb plane, as shown in Fig. 1(a), where the 3×3 supercell used to develop of our MLIP is displayed. Starting from this structure, we performed Bayesian active learning (BAL) using the Fast Learning of Atomistic Rare Events (FLARE) architecture [59] and Quantum Espresso (QE) [60–62] to provide reference electronic structure calculations. We ran several BAL trajectories at 300 K, collecting 265 frames to train the model. Further details are in the Supplementary information (SI) [63], with a summary of the workflow in Fig. 1(b).

As MLIP performance heavily depends on the hyperparameters, we conducted a hyperparameter scan (see SI). We found that a satisfactory value for r_{\max} , the interaction length scale in the model, is 5 Å; a reasonable compromise for l_{\max} , its spherical harmonics resolution, is 4; and for the number of layers (n_{layers}) of the neural network, describing the complexity of the interactions included, a value of 3 is sufficient. These hyperparameters are relatively standard choices except for $l_{\max} = 4$,

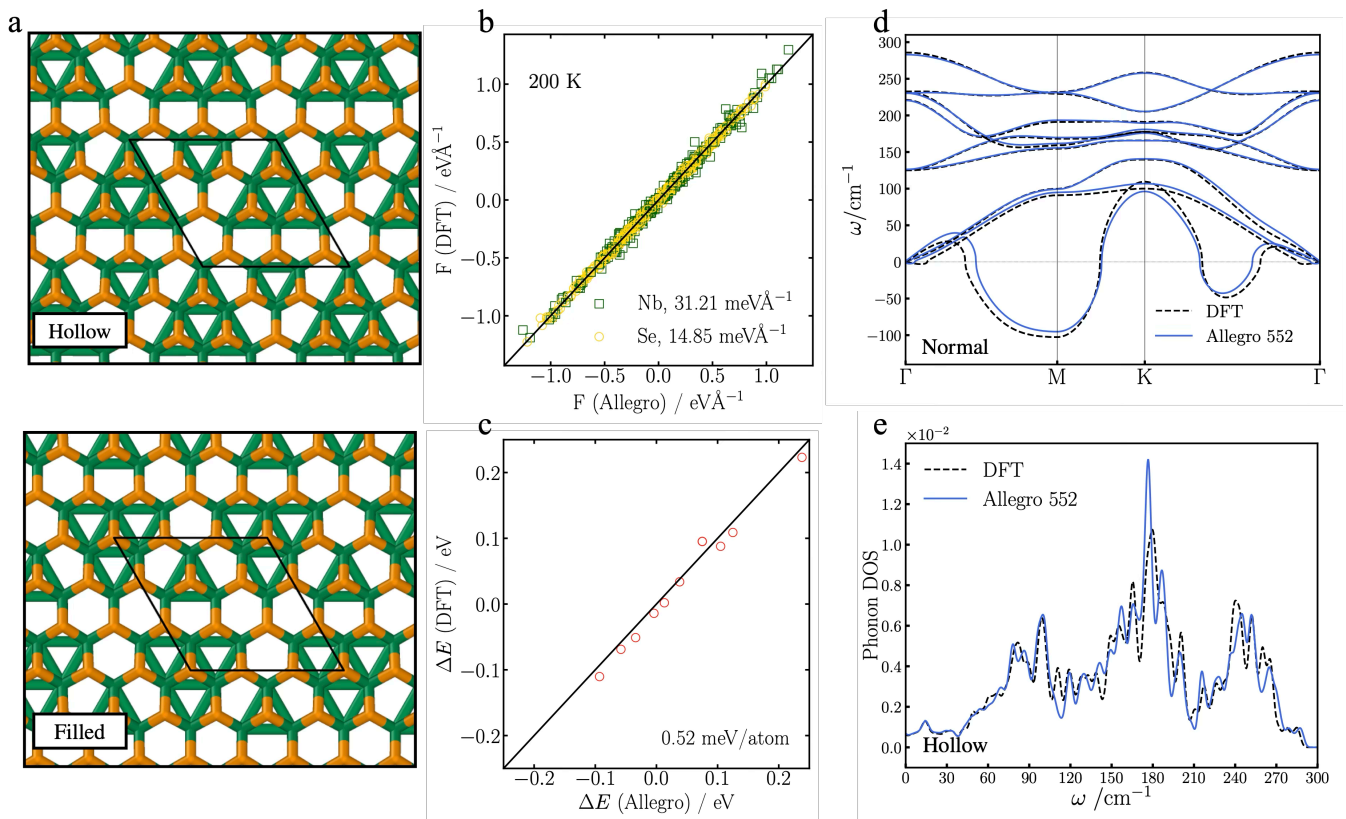


Figure 2: Development of a MLIP for NbSe₂ in the normal and CDW phases. **a** - Structure of the hollow (top) and filled (bottom) CDW phases of NbSe₂, with the 3×3 supercell shown. CDW distortions in the Nb atom positions are highlighted with additional sticks between Nb atoms, using a cutoff of 3.45 Å. **b** - Force MAE obtained from the Allegro MLIP predictions at 200 K in the NVT ensemble, compared with corresponding DFT values from Quantum ESPRESSO (QE). **c** - Corresponding energy MAE per simulation frame. **d** - Phonon dispersion curves for the normal phase, computed using DFT + Phonopy and Allegro MLIP + Phonopy, demonstrating close agreement. **e** - Phonon density of states at the Γ point for the hollow CDW phase, calculated from DFT + Phonopy and Allegro MLIP + Phonopy. See SI for additional computational details and discussion.

which is unusually large as required by the large density of d-states near the Fermi energy [57].

After selecting the hyperparameters, we tested our model by comparing the phonon dispersion from the trained MLIP with first-principles results (obtained via DFT and Phonopy [64], details in the SI), as shown in Fig. 1(c). We observed excellent agreement, with the largest deviation at the M-point. We then ran MD with this MLIP at 200 K, collecting structures, potential energies, and forces every 0.5 ps. These structures were used to compute the corresponding DFT ground-state, with the resulting parity plots shown in Figs. 1(d)-(e). We find excellent agreement between our MLIP and DFT, with a force mean absolute error (MAE) of 3.65 meVÅ⁻¹ for Se and 4.98 meVÅ⁻¹ for Nb, corresponding to an average force error of 1.4%, and an energy MAE of 0.04 meV/atom. In summary, we demonstrate that a satisfactory Allegro MLIP for monolayer NbSe₂ in the high temperature phase, i.e., without CDWs, can be developed with relatively little training data, and we move

on to investigating if Allegro can also capture the CDW phases.

Building on these results, we develop a model to study CDW phases under small-smearing conditions (low electronic temperatures). In these conditions, the symmetry-breaking transition creates a partial gap in the electronic band structure, driven by the competition between the energy cost associated with ionic lattice distortion and the gain in electronic energy as states are pushed to lower energies, stabilizing the CDW phases relative to the normal phase [30]. Fig. 2(a) shows the 3×3 CDW structure for the commonly observed ‘hollow’ and ‘filled’ phases, characterized by in-plane displacements of Nb atoms. DFT calculations reveal that the hollow and filled phases are 40 meV and 35 meV lower in energy than the normal phase, respectively, consistent with earlier findings [30]. With 27 atoms per unit cell, these energy differences correspond to ~ 1 meV/atom, setting the energy accuracy required to distinguish CDW phases from the normal state.

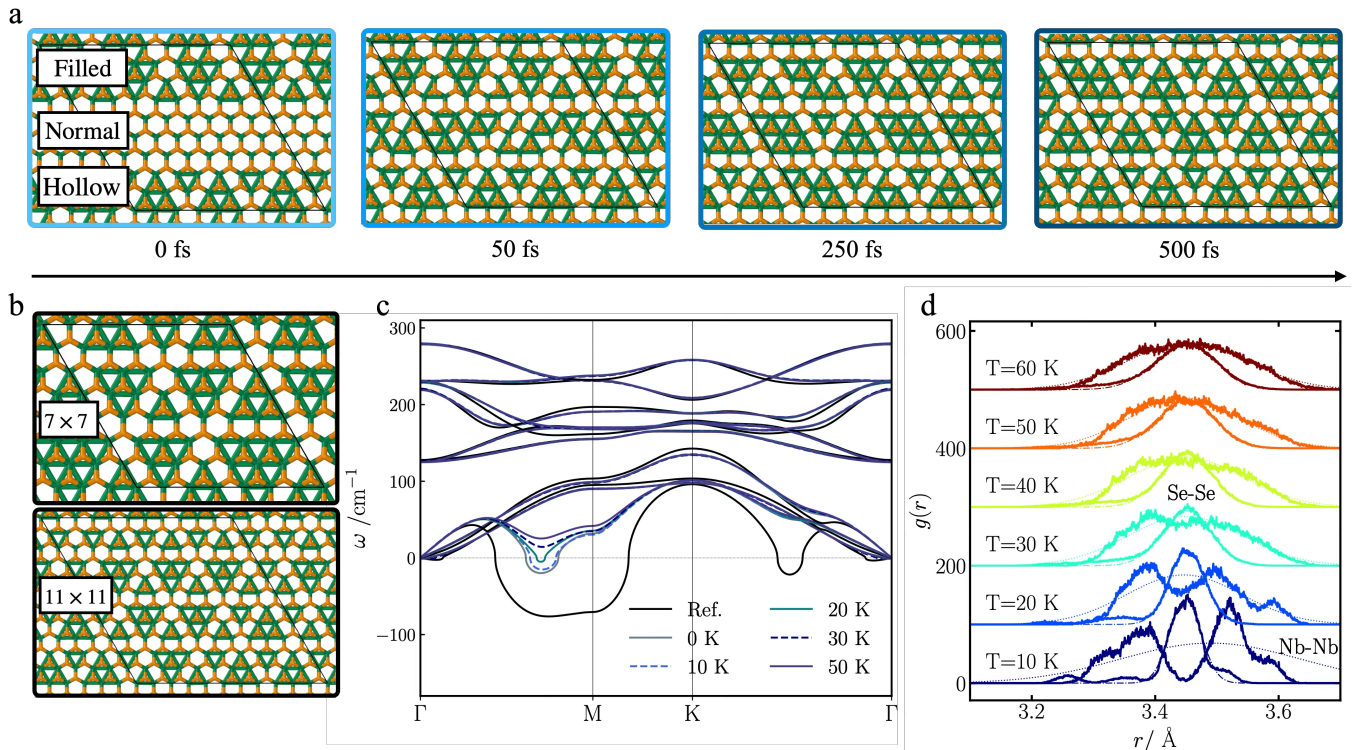


Figure 3: Results for the MLIP applied to NbSe_2 monolayers. **a** – MD NVT simulation at 10 K, starting from a 9×9 supercell prepared with a mixture of hollow, normal, and filled phases. Intermediate frames illustrate the system’s evolution during the relaxation process, with the final structure stabilizing in the hollow phase. **b** – Relaxation results for incommensurate supercells of NbSe_2 . The 7×7 supercell shows filled-phase features with some hollow distortions. The 11×11 supercell displays alternating filled/hollow 1×1 distortions, demonstrating the co-existence of hollow and filled CDW phases. **c** – Temperature-dependent phonon dispersion curves obtained using the self-consistent harmonic approximation (SSCHA) for the normal phase, illustrating the stabilization of the soft mode as temperature increases. For comparison, 0 K dispersions computed using Allegro MLIP + Phonopy (without SSCHA) are included and labeled as ‘Ref’. **d** – Pair correlation function obtained from classical MD simulations as a function of Nb-Nb and Se-Se distance for different temperatures, showing the transition from the normal state to the hollow CDW phase. See SI for additional details and discussion.

We first trained models using a dataset of 889 frames for the 3×3 monolayer, half generated via FLARE and half from relaxation after random displacements. The hyperparameter scan (see SI) identified $r_{\max} = 5 \text{ \AA}$, $l_{\max} = 5$, and $n_{\text{layers}} = 2$ as reasonable values. Again, large l_{\max} values produce satisfactory models, which is necessary because of the high density of d-states, especially with low-smearing [57]. Given that the CDW length scale is approximately 10.5 \AA , an $r_{\max} = 5 \text{ \AA}$ captures practically all of the environments. An $r_{\max} = 10 \text{ \AA}$ also performs well, but intermediate values showed poorer results. However, upon testing this ‘552’ model ($r_{\max} l_{\max} n_{\text{layers}}$) on supercells commensurate and incommensurate with the CDWs, we found that, respectively, the lowest energy structure deviated from the expected hollow/filled phase, and large energy and force errors occurred for all but the 1×1 structure, where the model extrapolated well. This breakdown in extensibility is particularly noteworthy, as it is often assumed that MLIPs can be directly applied to supercells of data they are

trained on, but our findings highlight that CDWs are a subtle phenomenon that requires more thorough training than most MLIPs applications.

To address these issues, we included 200 frames for the 3×3 monolayer under uniform strain ($\pm 1\%$, $\pm 2\%$) and 335 frames for incommensurate supercells (i.e., 1×1 , 2×2 , 4×4 , 5×5). The strained frames were generated through BAL, and the incommensurate ones through iterative learning from the previous Allegro model or from relaxations starting from random displacements. Including incommensurate supercells improved errors on these structures, albeit at the cost of reduced accuracy for the 3×3 supercells. Importantly, strained calculations helped mitigate ripple effects in larger supercells (e.g., 10×10). Overall, incorporating both strained and incommensurate structures is essential for robust modeling of CDWs in NbSe_2 (see SI).

To validate the final model, we compared the phonon predictions from MLIP with DFT results for the normal (1×1) and hollow CDW (3×3) phases (Figs. 2(d)-

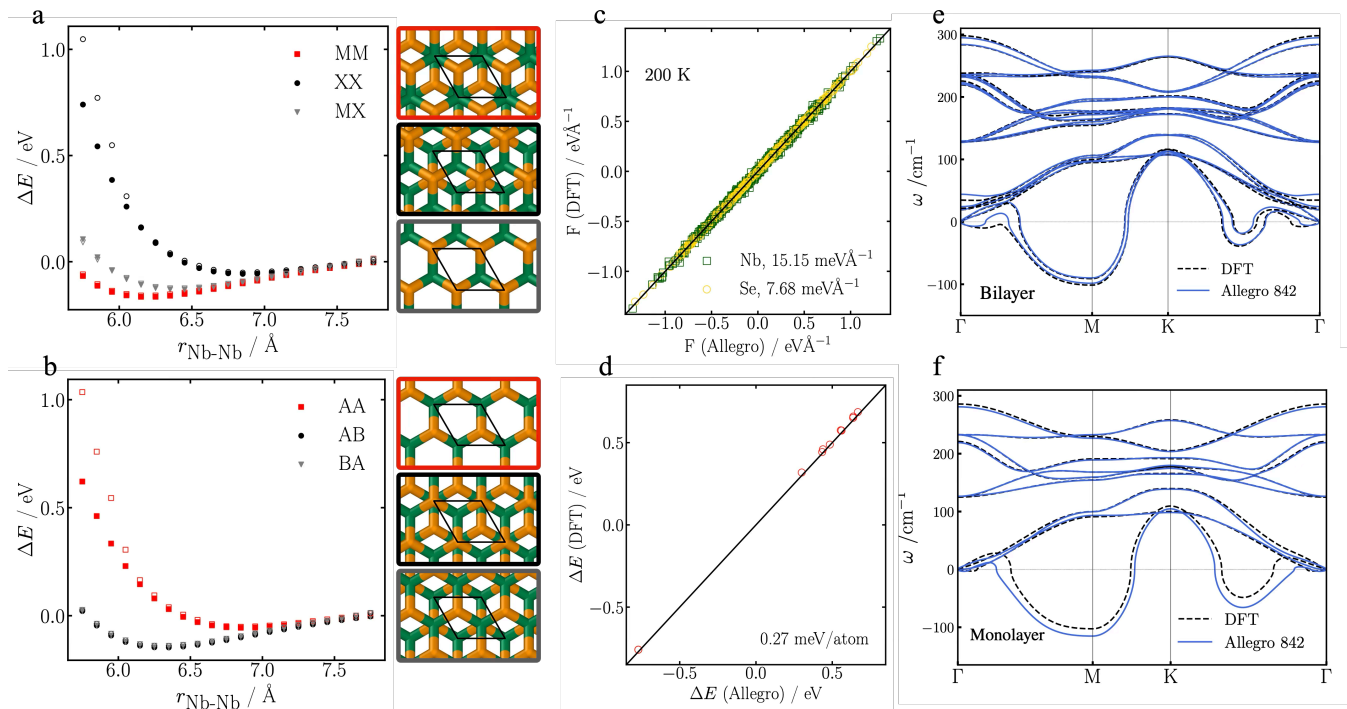


Figure 4: Development of a MLIP for bilayer NbSe₂. **a** - Binding energy curves for high-symmetry stackings of the 180° NbSe₂ bilayer. Filled symbols represent Allegro MLIP results, and empty symbols represent DFT results. **b** - Binding energy curves for high-symmetry stackings of the 0° NbSe₂ bilayer. Filled symbols represent Allegro MLIP results, and empty symbols represent DFT results. **c** - Force MAE obtained from running the Allegro MLIP at 200 K in NVT, collecting structures, forces, and energies, and comparing these with corresponding values from DFT using QE. **d** - Corresponding energy MAE per simulation frame. **e** - Phonon dispersion curves for the normal phase of the bilayer in the MM stacking. A comparison is shown between DFT + Phonopy and Allegro MLIP + Phonopy. **f** Phonon dispersion curves for the normal phase of the monolayer, using the bilayer MLIP. A comparison is shown between DFT + Phonopy and Allegro MLIP + Phonopy. See SI for additional computational details.

(e)). Throughout this work, the phonon dispersions of the normal phase (except for SSCHA calculations) were computed on a 3×3 supercell. Although not fully converged, this provides a consistent comparison between DFT and Allegro (see SI). As expected, the normal phase exhibited an unstable acoustic phonon mode, indicative of a CDW instability, with negative frequencies around Γ -M and M-K. [9, 11, 18] Overall, the phonon dispersions agree well across the Brillouin zone, including the unstable mode. Notably, we observed a discrepancy between finite-difference methods (MLIP or DFT with Phonopy) and density-functional perturbation theory (DFPT) [65, 66], where finite-difference methods showed an additional instability between K- Γ not seen in DFPT (see SI). This appears to be a consequence of subtle numerical approximation differences between the finite difference and perturbative methods, even on the DFT level, that warrants further investigation, though it is beyond the scope of this study. For the hollow phase (Fig. 2(e)), the phonon density of states obtained from MLIP and DFT agree remarkably well, likely due to the absence of the unstable mode.

Further, we performed MD simulations at 200 K us-

ing the NVT ensemble with our MLIP and compared the resulting energies and forces against DFT (Figs. 2(b)-(c)). The model showed good agreement with a force MAE of 14.85 meV/Å for Se and 31.21 meV/Å for Nb and an energy MAE of 0.52 meV/atom. While the errors are slightly larger than in the large-smearing case, the dataset here is notably more challenging, with force errors around $\sim 5\%$. Further parity plots for incommensurate structures are provided in the SI.

Having established our model’s accuracy, we now explore CDWs in monolayer NbSe₂. In Fig. 3(a), we show the evolution of the CDWs in MD at 10 K (NVT), starting from a configuration with coexisting hollow, normal, and filled phases. After ~ 50 fs, the regions initially in the normal state have CDW-like distortions resembling both the hollow and filled phases, while the original hollow/filled regions remain largely unchanged. At ~ 250 fs, the region that was initially in the normal phase predominantly exhibits hollow-like CDW distortions, and the hollow/filled regions remain largely unchanged. Finally, after ~ 450 fs all regions have converted to hollow-dominated CDW features, though the originally filled region retains more filled-like features. At longer times, the

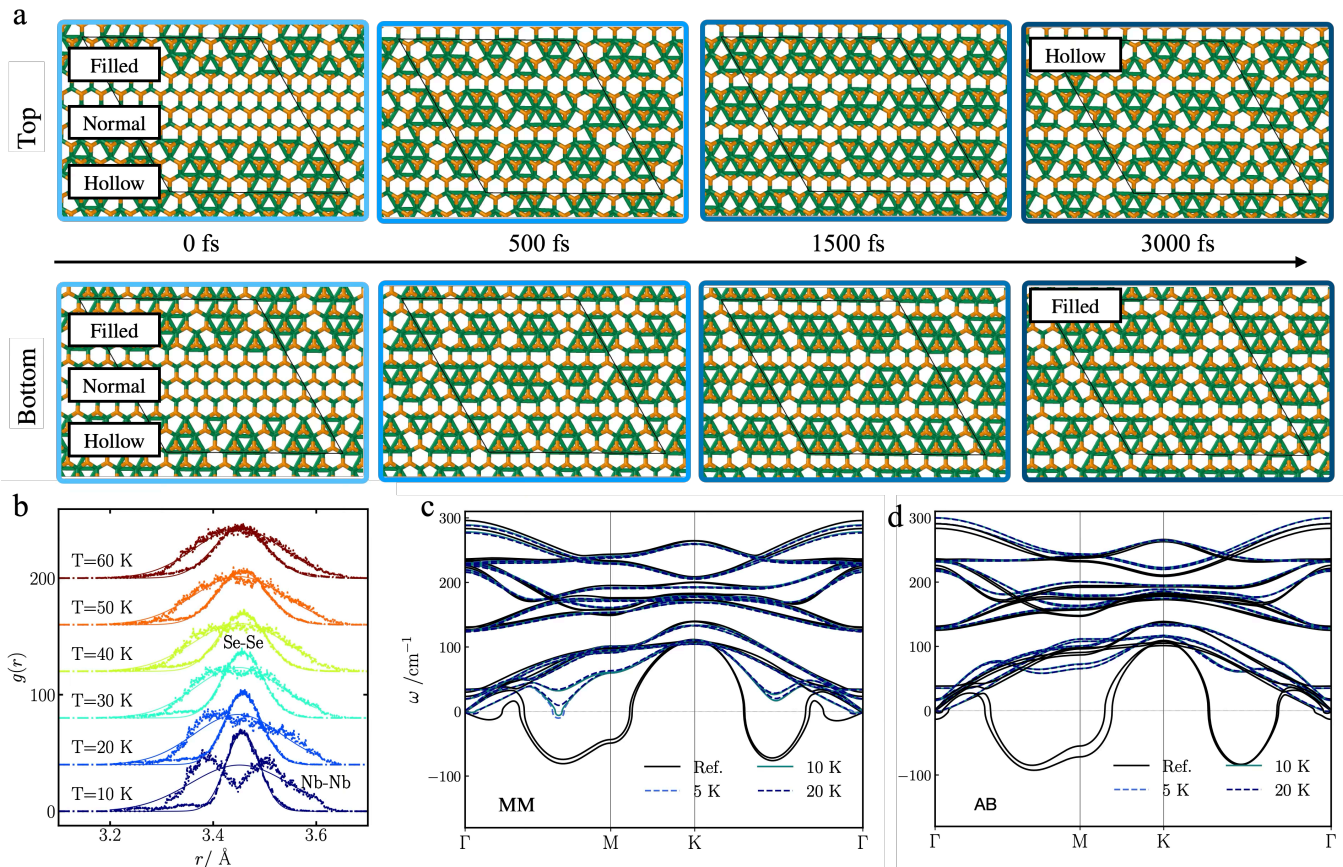


Figure 5: Results for the MLIP applied to NbSe₂ bilayers. **a** – MD NVT simulation at 10 K, starting from a 9×9 supercell prepared with a mixture of hollow, normal, and filled phases in both layers. Intermediate frames illustrate the evolution of the system during the relaxation process, with the final structure corresponding to the stable configuration. **b** – Pair correlation function obtained via classical MD simulations as a function of Nb-Nb distances for different temperatures, showing the transition to the charge density wave (CDW) phase, with hollow plane and filled plane structures. **c** – SSCHA temperature-dependent phonon dispersion curves for the bilayer in the normal phase, MM stacking, illustrating how the soft mode stabilizes with increasing temperature. For comparison, 0 K dispersions computed using Allegro + Phonopy (without SSCHA) are included and labeled as ‘Ref’. **d** – Same as (c), but for AB stacking. Again, for comparison, 0 K dispersions computed using Allegro + Phonopy (without SSCHA) are included and labeled as ‘Ref’. See Supporting SI for additional details and discussion.

supercell becomes purely hollow-like, as expected [30].

So far, we have tested our model on supercells commensurate with CDWs (e.g., 3×3 or multiples thereof), which capture the periodic distortion. However, modeling CDWs sometimes requires incommensurate supercells (e.g., moiré patterns, substrates), and accurate transferability is not guaranteed due to finite-size effects. Fig. 3(b) shows relaxations for 7×7 and 11×11 supercells. The 7×7 structure mainly exhibits features reminiscent of the filled phase, with some hollow features also present, corresponding to the larger 2×2 triangular distortions seen in the pristine phases. The 11×11 structure shows alternating filled/hollow triangular distortions in the top row and left-most column, with the remainder tessellated with filled and hollow phases. Overall, our model revealed coexisting hollow/filled phases in incommensurate

supercells, suggesting that the coexistence of CDWs in twisted bilayers of NbSe₂ could originate from the incommensurate structures. [46]

Beyond CDW structures, our model provides insight into CDW transition temperatures (T_{CDW}). Estimating T_{CDW} requires accurately capturing anharmonic effects, delicate total energy changes due structural distortions, and vibrational excitations. Classical MD does not fully describe vibrational entropy contributions due to quantized fluctuations [11, 67]. To address this, we employed SSCHA [68, 69] with our Allegro-MLIP to compute temperature-dependent phonon dispersions and identify the temperature at which the soft mode stabilizes. As shown in Fig. 3(c), phonon dispersions soften near 30 K ($q_{\text{CDW}} = 2/3 \Gamma\text{-M}$, corresponding to a 3×3 distortion) and become negative at 20 K, placing T_{CDW}

in the 20-30 K range. This is lower than previous SSCHA estimates [11] of 73 K, but aligns closely with STM measurements [29].

Notably, T_{CDW} estimates from Allegro+SSCHA are highly sensitive to DFT settings, including lattice parameters and exchange-correlation functional approximations used for training, as well as the MLIP fidelity, due to the small energy differences ($\sim 1\text{meV}/\text{atom}$) between the CDW and normal states [70, 71]. Variations between finite-difference methods and DFPT in capturing the unstable mode may also contribute to discrepancies with experiments.

For comparison, classical MD simulations predict $T_{\text{CDW}} \approx 30\text{--}40\text{ K}$, consistent with both SSCHA and STM. This estimate is inferred from the pair correlation functions $g(r)$ for Nb–Nb and Se–Se distances becoming unimodal near 40 K—while at 30 K, the Nb–Nb distribution remains clearly bimodal. Structural analysis showed that the hollow phase remains stable up to 15–20 K, exhibiting only fluctuations. At higher temperatures, the structure transitions dynamically among hollow, filled, and hexagonal configurations. Whereas, starting from the filled phase, it survives up to 5–10 K, rapidly converting to the hollow structure at higher temperature and then exhibiting the temperature-dependent behavior of the hollow phase. These results demonstrate that our MLIP, combined with either SSCHA or classical MD, enables efficient exploration of T_{CDW} —a task prohibitively expensive with *ab initio* MD, and even more so with path integral MD.

As monolayer NbSe₂ is experimentally challenging to fabricate and measure, we extend our dataset to enable predictions for bilayer structures. The new dataset consists of 1496 BAL-generated structures, including 471 monolayer frames from the previous dataset and 1025 bilayer frames from five stackings with varying interlayer distances at 0° and 180°. We performed the hyperparameter scan (see SI) and identified $r_{\text{max}} = 8\text{ \AA}$, $l_{\text{max}} = 4$ and $n_{\text{layers}} = 2$ as optimal values. The key adjustment arises from the equilibrium interlayer distance between Nb atoms ($\approx 6.5\text{ \AA}$), requiring $r_{\text{max}} = 8\text{ \AA}$ to capture the interlayer coupling critical for predicting CDW reconstructions.

First, we compared model and DFT binding energy curves for the indicated stackings (Figs. 4(a)-(b)), finding good agreement with minor discrepancies at extreme interlayer distances not thoroughly explored by BAL. Next, we compared the energy and forces for the most stable MM stacking from MD simulations at 200 K (NVT). As shown in Figs. 4(c)-(d), the energy and forces errors are even smaller than for the monolayer, confirming the model’s accuracy.

The phonon spectrum for the MM stacking (Fig. 4(e)) shows good agreement between DFT and MLIP, with minor discrepancies in the unstable and higher-energy optical modes. The bilayer phonon modes resemble those of the monolayer in the normal phase (Fig. 4(f)), with each mode nearly doubly degenerate due to the relatively weak

van der Waals coupling. Our unified model accurately describes the phonons of both monolayers and bilayers using the same dataset and hyperparameters.

To explore CDWs in bilayers, we applied our model to a system with coexisting CDW/normal phases in both layers. Specifically, we initialized the normal, hollow, and filled phases in each layer within a 9×9 supercell, as shown in Fig. 5(a). Running MD at 10 K, we consistently observed one layer becoming a filled CDW and the other a hollow CDW. This mixed-phase configuration was also observed in AB stacking (see SI), confirming its energetic favourability—at least among the low-energy stackings—and aligning with recent DFT results [46]. Notably, the bilayer took significantly longer to relax into the hollow/filled configuration compared to the monolayer reaching its CDW minimum, i.e., the hollow phase. While the hollow layer remained nearly pristine, the filled layer showed deviations from the ideal filled CDW, consistent with monolayer dynamics observed when starting from the filled phase at 10 K. Moreover, directly relaxing the coexistence-initialized structure—without annealing—led to a local minimum distinct from the observed hollow/filled state, emphasizing the importance of annealing in capturing the correct bilayer ground state.

Finally, we estimate T_{CDW} from SSCHA phonon spectra. As shown in Fig. 5(c), the transition temperature for the MM stacking slightly decreases compared to the monolayer, falling in the 10–20 K range, consistent with classical MD estimates (Fig. 5(b)). In contrast, Fig. 5(d) shows that for the AB stacking, the CDW is suppressed at 5 K, highlighting the impact of stacking on CDW stability. The MM stacking results align with previous work [11], which reported a weak dimensionality dependence of T_{CDW} relative to the bulk, although our absolute values are lower than both earlier theoretical predictions and experimental measurements. In classical MD, $g(r)$ becomes unimodal around 20 K; however, the mixed hollow/filled CDW configuration remains stable only up to $\approx 5\text{ K}$, beyond which the filled layer exhibited dynamic fluctuations.

In summary, we present a robust and transferable machine learning protocol for studying CDWs in 2D NbSe₂, broadly applicable to other layered systems exhibiting similar phenomena. For monolayers, we show that accurate MLIPs can be trained on relatively small datasets (~ 1000 frames), especially by combining BAL with random displacement relaxations to maximize configuration diversity. Incorporating strained and incommensurate structures significantly enhances model transferability and extensibility. Using this model, we investigated CDW reconstructions and estimated critical temperatures. SSCHA predicts T_{CDW} in the 20–30 K range, in close agreement with classical MD and STM measurements [29], with hollow phases dominating at 10 K. While the SSCHA+MLIP approach captures key trends, its sensitivity to the small energy differences between phases requires caution when comparing to experiments. Incommensurate structures tend to exhibit coexisting

hollow/filled-like features. For bilayers, expanding the dataset improves accuracy, though balancing dataset size with computational efficiency remains crucial. SSCHA reveals weak dimensionality dependence, with T_{CDW} decreasing to 10–20 K for MM stacking, consistent with MD and prior studies [11, 29]. Notably, MM-stacked bilayers consistently relax into mixed hollow–filled CDW states. Our approach provides a foundation for investigating CDW evolution across different stackings and layer numbers, with direct relevance to multilayer and twisted systems. Future work incorporating doping and substrate interactions will broaden the model’s applicability to increasingly complex experimental systems.

ACKNOWLEDGMENTS

We thank Cameron Owen and Stefano Falletta for stimulating discussions. N.R. acknowledges support

through the the Enterprise Science Fund (Project 218056— Twisted NbSe₂). Computational resources are provided for by Harvard FAS Research Computing. Z.A.H.G acknowledges support through the Glaxstone Research Fellowship in Materials, University of Oxford. F.L. acknowledges support through the Swiss National Science Foundation (SNSF) mobility fellowship P500PT_217861. A.O.F and J.L.L. acknowledge the computational resources provided by the Aalto Science-IT project and the financial support from Finnish Quantum Flagship, InstituteQ, the Jane and Aatos Erkkö Foundation and the Academy of Finland Projects Nos. 331342, 358088, and 349696. C. T. S. C. acknowledges funding from the Croucher Foundation and an Imperial College President’s Scholarship. This work used the ARCHER2 UK National Supercomputing Service (<https://www.archer2.ac.uk>) and the Imperial College Research Computing Service facility CX1 (DOI: 10.14469/hpc/2232). We acknowledge the Thomas Young Centre under Grant No. TYC-101.

-
- [1] M. M. Ugeda, A. J. Bradley, Y. Zhang, S. Onishi, Y. Chen, W. Ruan, C. Ojeda-Aristizabal, H. Ryu, M. T. Edmonds, H.-Z. Tsai, *et al.*, Characterization of collective ground states in single-layer NbSe₂, *Nat. Phys.* **12**, 92 (2016).
- [2] X. Xi, L. Zhao, Z. Wang, H. Berger, L. Forró, J. Shan, and K. F. Mak, Strongly enhanced charge-density-wave order in monolayer NbSe₂, *Nat. Nanotechnol* **10**, 765 (2015).
- [3] C.-S. Lian, C. Si, J. Wu, and W. Duan, First-principles study of Na-intercalated bilayer NbSe₂: Suppressed charge-density wave and strain-enhanced superconductivity, *Phys. Rev. B* **96**, 235426 (2017).
- [4] H. Zhang, A. Rousuli, K. Zhang, L. Luo, C. Guo, X. Cong, Z. Lin, C. Bao, H. Zhang, S. Xu, *et al.*, Tailored ising superconductivity in intercalated bulk NbSe₂, *Nat. Phys.* **18**, 1425 (2022).
- [5] D. Lin, S. Li, J. Wen, H. Berger, L. Forró, H. Zhou, S. Jia, T. Taniguchi, K. Watanabe, X. Xi, *et al.*, Patterns and driving forces of dimensionality-dependent charge density waves in 2 h-type transition metal dichalcogenides, *Nature communications* **11**, 2406 (2020).
- [6] Y. Nakata, K. Sugawara, S. Ichinokura, Y. Okada, T. Hitosugi, T. Koretsune, K. Ueno, S. Hasegawa, T. Takahashi, and T. Sato, Anisotropic band splitting in monolayer NbSe₂: implications for superconductivity and charge density wave, *npj 2D Mater. Appl.* **2**, 12 (2018).
- [7] X. Xi, Z. Wang, W. Zhao, J.-H. Park, K. T. Law, H. Berger, L. Forró, J. Shan, and K. F. Mak, Ising pairing in superconducting nbse 2 atomic layers, *Nat. Phys.* **12**, 139 (2016).
- [8] P. Baidya, D. Sahani, H. K. Kundu, S. Kaur, P. Tiwari, V. Bagwe, J. Jesudasan, A. Narayan, P. Raychaudhuri, and A. Bid, Transition from three-to two-dimensional ising superconductivity in few-layer NbSe₂ by proximity effect from van der waals heterostacking, *Phys. Rev. B* **104**, 174510 (2021).
- [9] M. Calandra, I. Mazin, and F. Mauri, Effect of dimensionality on the charge-density wave in few-layer 2H-NbSe₂, *Phys. Rev. B* **80**, 241108 (2009).
- [10] M. Leroux, M. Le Tacon, M. Calandra, L. Cario, M. A. Measson, P. Diener, E. Borrisenko, A. Bosak, and P. Rodiere, Anharmonic suppression of charge density waves in 2H-Nbse₂, *Phys. Rev B* **86**, 155125 (2012).
- [11] R. Bianco, L. Monacelli, M. Calandra, F. Mauri, and I. Errea, Weak dimensionality dependence and dominant role of ionic fluctuations in the charge-density-wave transition of NbSe₂, *Phys. Rev. Lett.* **125**, 106101 (2020).
- [12] J. A. Silva-Guillén, P. Ordejón, F. Guinea, and E. Canadell, Electronic structure of 2H-NbSe₂ single-layers in the CDW state, *2D Mater* **3**, 035028 (2016).
- [13] R. Peierls, Zur theorie der elektrischen und thermischen leitfähigkeit von metallen, *Annalen der Physik* **396**, 121 (1930).
- [14] R. E. Peierls, *Quantum theory of solids* (Clarendon Press, 1996).
- [15] J. Luttinger, An exactly soluble model of a many-fermion system, *Journal of mathematical physics* **4**, 1154 (1963).
- [16] J.-P. Pouget, The peierls instability and charge density wave in one-dimensional electronic conductors, *Comptes Rendus Physique* **17**, 332 (2016).
- [17] F. Weber, S. Rosenkranz, J.-P. Castellán, R. Osborn, R. Hott, R. Heid, K.-P. Bohnen, T. Egami, A. Said, and D. Reznik, Extended phonon collapse and the origin of the charge-density wave in 2H-NbSe₂, *Phys. Rev. Lett.* **107**, 107403 (2011).
- [18] F. Zheng and J. Feng, Electron-phonon coupling and the coexistence of superconductivity and charge-density wave in monolayer NbSe₂, *Phys. Rev. B* **99**, 161119 (2019).
- [19] A. Hamill, B. Heischmidt, E. Sohn, D. Shaffer, K.-T. Tsai, X. Zhang, X. Xi, A. Suslov, H. Berger, L. Forró, *et al.*, Two-fold symmetric superconductivity in few-layer NbSe₂, *Nat. Phys.* **17**, 949 (2021).
- [20] D. Wickramaratne, S. Khmelevskiy, D. F. Agterberg, and I. Mazin, Ising superconductivity and magnetism in

- NbSe₂, *Phys. Rev. X* **10**, 041003 (2020).
- [21] E. Khestanova, J. Birkbeck, M. Zhu, Y. Cao, G. Yu, D. Ghazaryan, J. Yin, H. Berger, L. Forro, T. Taniguchi, *et al.*, Unusual suppression of the superconducting energy gap and critical temperature in atomically thin NbSe₂, *Nano Lett.* **18**, 2623 (2018).
- [22] K. Cho, M. Kończykowski, S. Teknowijoyo, M. A. Tanatar, J. Guss, P. Gartin, J. Wilde, A. Kreyssig, R. McQueeney, A. I. Goldman, *et al.*, Using controlled disorder to probe the interplay between charge order and superconductivity in NbSe₂, *Nat. Commun.* **9**, 2796 (2018).
- [23] C. Chen, P. Das, E. Aytan, W. Zhou, J. Horowitz, B. Satpati, A. A. Balandin, R. K. Lake, and P. Wei, Strain-controlled superconductivity in few-layer NbSe₂, *ACS Appl. Mater. Interfaces.* **12**, 38744 (2020).
- [24] X. Xi, H. Berger, L. Forró, J. Shan, and K. F. Mak, Gate tuning of electronic phase transitions in two-dimensional NbSe₂, *Phys. Rev. Lett.* **117**, 106801 (2016).
- [25] J. Li, W. Ma, L. Jiang, N. Yao, J. Deng, Q. Qiu, Y. Shi, W. Zhou, and Z. Huang, High performance of room-temperature NbSe₂ terahertz photoelectric detector, *ACS Appl. Mater. Interfaces.* **14**, 14331 (2022).
- [26] Y. Ding, C. Hu, W. Li, L. Chen, J. He, Y. Zhang, X. Zeng, Y. Wang, P. Dong, J. Wang, *et al.*, Gate-controlled superconducting switch in GaSe/NbSe₂ van der waals heterostructure, *ACS nano* (2025).
- [27] T. Dvir, A. Zalic, E. H. Fyhn, M. Amundsen, T. Taniguchi, K. Watanabe, J. Linder, and H. Steinberg, Planar graphene-NbSe₂ josephson junctions in a parallel magnetic field, *Phys. Rev. B* **103**, 115401 (2021).
- [28] G. Gruner, *Density waves in solids* (CRC press, 2018).
- [29] C. J. Arguello, S. P. Chockalingam, E. P. Rosenthal, L. Zhao, C. Gutiérrez, J. Kang, W. Chung, R. M. Fernandes, S. Jia, A. J. Millis, *et al.*, Visualizing the charge density wave transition in 2H-NbSe₂ in real space, *Phys. Rev. B* **89**, 235115 (2014).
- [30] C.-S. Lian, C. Si, and W. Duan, Unveiling charge-density wave, superconductivity, and their competitive nature in two-dimensional NbSe₂, *Nano Lett.* **18**, 2924 (2018).
- [31] F. Cossu, A. G. Moghaddam, K. Kim, H. A. Tahini, I. Di Marco, H.-W. Yeom, and A. Akbari, Unveiling hidden charge density waves in single-layer nbse 2 by impurities, *Physical Review B* **98**, 195419 (2018).
- [32] B. Guster, C. Rubio-Verdú, R. Robles, J. Zaldívar, P. Dreher, M. Pruneda, J. Á. Silva-Guillén, D.-J. Choi, J. I. Pascual, M. M. Ugeda, *et al.*, Coexistence of elastic modulations in the charge density wave state of 2H-NbSe₂, *Nano Lett.* **19**, 3027 (2019).
- [33] F. Cossu, D. Nafday, K. Palotás, M. Biderang, H.-S. Kim, A. Akbari, and I. Di Marco, Stacking of charge-density waves in 2H-NbSe₂ bilayers, *Phys. Rev. Research* **6**, 043111 (2024).
- [34] P. Dreher, W. Wan, A. Chikina, M. Bianchi, H. Guo, R. Harsh, S. Manñas Valero, E. Coronado, A. J. Martínez-Galera, P. Hofmann, *et al.*, Proximity effects on the charge density wave order and superconductivity in single-layer NbSe₂, *ACS Nano* **15**, 19430 (2021).
- [35] S. Carr, D. Massatt, S. Fang, P. Cazeaux, M. Luskun, and E. Kaxiras, Twistrionics: Manipulating the electronic properties of two-dimensional layered structures through their twist angle, *Pys. Rev. B* **95**, 075420 (2017).
- [36] Y. Cao, V. Fatemi, A. Demir, S. Fang, S. L. Tomarken, J. Y. Luo, J. D. Sanchez-Yamagishi, K. Watanabe, T. Taniguchi, E. Kaxiras, R. C. Ashoori, and P. Jarillo-Herrero, Correlated insulator behaviour at half-filling in magic-angle graphene superlattices, *Nature* **556**, 80 (2018).
- [37] Y. Cao, V. Fatemi, S. Fang, K. Watanabe, T. Taniguchi, E. Kaxiras, and P. Jarillo-Herrero, Unconventional superconductivity in magic-angle graphene superlattices, *Nature* **556**, 43 (2018).
- [38] A. Kerelsky, L. J. McGilly, D. M. Kennes, L. Xian, M. Yankowitz, S. Chen, K. Watanabe, T. Taniguchi, J. Hone, C. Dean, *et al.*, Maximized electron interactions at the magic angle in twisted bilayer graphene, *Nature* **572**, 95 (2019).
- [39] Z. Hao, A. M. Zimmerman, P. Ledwith, E. Khalaf, D. H. Najafabadi, K. Watanabe, T. Taniguchi, A. Vishwanath, and P. Kim, Electric field-tunable superconductivity in alternating-twist magic-angle trilayer graphene, *Science* **371**, 1133 (2021).
- [40] J. M. Park, Y. Cao, L.-Q. Xia, S. Sun, K. Watanabe, T. Taniguchi, and P. Jarillo-Herrero, Robust superconductivity in magic-angle multilayer graphene family, *Nat. Mater.* **21**, 877 (2022).
- [41] N. Zhang, A. Surrente, M. Baranowski, D. K. Maude, P. Gant, A. Castellanos-Gomez, and P. Plochocka, Moiré intralayer excitons in a MoSe₂/MoS₂ heterostructure, *Nano Lett.* **18**, 7651 (2018).
- [42] M. R. Rosenberger, H.-J. Chuang, M. Phillips, V. P. Oleshko, K. M. McCreary, S. V. Sivaram, C. S. Hellberg, and B. T. Jonker, Twist angle-dependent atomic reconstruction and moiré patterns in transition metal dichalcogenide heterostructures, *ACS nano* **14**, 4550 (2020).
- [43] K. F. Mak and J. Shan, Semiconductor moiré materials, *Nature Nanotechnology* **17**, 686 (2022).
- [44] D. M. Kennes, M. Claassen, L. Xian, A. Georges, A. J. Millis, J. Hone, C. R. Dean, D. N. Basov, A. N. Pasupathy, and A. Rubio, Moiré heterostructures as a condensed-matter quantum simulator, *Nat. Phys.* **17**, 155 (2021).
- [45] Z. A. Goodwin and V. I. Fal'ko, Moiré modulation of charge density waves, *Journal of Physics: Condensed Matter* **34**, 494001 (2022).
- [46] C. T. S. Cheung, Z. A. H. Goodwin, Y. Han, J. Lu, and A. A. M. and Johannes Lischner, Coexisting charge density waves in twisted bilayer NbSe₂, *Nano Lett.* **24**, 12088 (2024).
- [47] J. Behler, Four generations of high-dimensional neural network potentials, *Chem. Rev.* **121**, 10037 (2021).
- [48] V. L. Deringer, M. A. Caro, and G. Csányi, Machine learning interatomic potentials as emerging tools for materials science, *Adv. Mater.* **31**, 1902765 (2019).
- [49] V. L. Deringer, A. P. Bartók, N. Bernstein, D. M. Wilkins, M. Ceriotti, and G. Csányi, Gaussian process regression for materials and molecules, *Chem. Rev.* **121**, 10073 (2021).
- [50] S. Falletta, A. Cepellotti, C. W. Tan, A. Johansson, A. Musaelian, C. J. Owen, and B. Kozinsky, Unified differentiable learning of the electric enthalpy and dielectric properties with exact physical constraints, *arXiv:2403.17207* (2024).
- [51] Z. A. Goodwin, M. B. Wenny, J. H. Yang, A. Cepellotti, J. Ding, K. Bystrom, B. R. Duschatko, A. Johansson, L. Sun, S. Batzner, A. Musaelian, J. A. Mason,

- B. Kozinsky, and N. Molinari, Transferability and accuracy of ionic liquid simulations with equivariant machine learning interatomic potentials, *J Phys. Chem. Lett.* **15**, 7539 (2024).
- [52] P. Rowe, G. Csányi, D. Alfè, and A. Michaelides, Development of a machine learning potential for graphene, *Phys. Rev. B* **97**, 054303 (2018).
- [53] F. L. Thiemann, P. Rowe, E. A. Müller, and A. Michaelides, Machine learning potential for hexagonal boron nitride applied to thermally and mechanically induced rippling, *J. Phys. Chem. C* **124**, 22278 (2020).
- [54] A. Siddiqui and N. D. M. Hine, Machine-learned interatomic potentials for transition metal dichalcogenide $\text{Mo}_{1-x}\text{W}_x\text{S}_{2-2y}\text{Se}_{2y}$ alloys, *npj Comput. Mater.* **10**, 169 (2024).
- [55] A. Stukowski, Visualization and analysis of atomistic simulation data with ovito—the open visualization tool, *Model. Simul. Mater. Sci. Eng* **18**, 015012 (2009).
- [56] A. Musaelian, S. Batzner, A. Johansson, L. Sun, C. J. Owen, M. Kornbluth, and B. Kozinsky, Learning local equivariant representations for large-scale atomistic dynamics, *Nat. Commun.* **14**, 579 (2023).
- [57] C. J. Owen, S. B. Torrisi, Y. Xie, S. Batzner, K. Bystrom, J. Coulter, A. Musaelian, L. Sun, and B. Kozinsky, Complexity of many-body interactions in transition metals via machine-learned force fields from the TM23 data set, *npj Comput. Mater.* **10**, 92 (2024).
- [58] S. Batzner, A. Musaelian, L. Sun, M. Geiger, J. P. Mailoa, M. Kornbluth, N. Molinari, T. E. Smidt, and B. Kozinsky, E(3)-equivariant graph neural networks for data-efficient and accurate interatomic potentials, *Nat. Commun.* **13**, 2453 (2022).
- [59] J. Vandermause, S. B. Torrisi, S. Batzner, Y. Xie, L. Sun, A. M. Kolpak, and B. Kozinsky, On-the-fly active learning of interpretable bayesian force fields for atomistic rare events, *npj Comput. Mater.* **6**, 20 (2020).
- [60] P. Giannozzi, S. De Gironcoli, P. Pavone, and S. Baroni, Ab initio calculation of phonon dispersions in semiconductors, *Phys. Rev. B* **43**, 7231 (1991).
- [61] P. Giannozzi, O. Andreussi, T. Brumme, O. Bunau, M. B. Nardelli, M. Calandra, R. Car, C. Cavazzoni, D. Ceresoli, M. Cococcioni, *et al.*, Advanced capabilities for materials modelling with quantum espresso, *J Phys.: Condens. matter* **29**, 465901 (2017).
- [62] P. Giannozzi, S. Baroni, N. Bonini, M. Calandra, R. Car, C. Cavazzoni, D. Ceresoli, G. L. Chiarotti, M. Cococcioni, I. Dabo, *et al.*, Quantum espresso: a modular and open-source software project for quantum simulations of materials, *Journal of physics: Condensed matter* **21**, 395502 (2009).
- [63] Supplementary information, Online.
- [64] A. Togo, First-principles phonon calculations with phonopy and phono3py, *Journal of the Physical Society of Japan* **92**, 012001 (2023).
- [65] X. Gonze and C. Lee, Dynamical matrices, born effective charges, dielectric permittivity tensors, and interatomic force constants from density-functional perturbation theory, *Phys. Rev. B* **55**, 10355 (1997).
- [66] S. Baroni, S. De Gironcoli, A. Dal Corso, and P. Giannozzi, Phonons and related crystal properties from density-functional perturbation theory, *Rev. Mod. Phys.* **73**, 515 (2001).
- [67] R. Bianco, I. Errea, L. Monacelli, M. Calandra, and F. Mauri, Quantum enhancement of charge density wave in NbS_2 in the two-dimensional limit, *Nano Lett.* **19**, 3098 (2019).
- [68] L. Monacelli, R. Bianco, M. Cherubini, M. Calandra, I. Errea, and F. Mauri, The stochastic self-consistent harmonic approximation: calculating vibrational properties of materials with full quantum and anharmonic effects, *J. Phys.: Condens. Matter* **33**, 363001 (2021).
- [69] R. Bianco, I. Errea, L. Paulatto, M. Calandra, and F. Mauri, Second-order structural phase transitions, free energy curvature, and temperature-dependent anharmonic phonons in the self-consistent harmonic approximation: Theory and stochastic implementation, *Phys. Rev. B* **96**, 014111 (2017).